Biology and Medicine

Inhibition of PKC β Mediates Cardioprotective Activity of Ambrex against Isoproterenol-Induced Myocardial Necrosis: *in vivo* and *in silico* Studies

Rekha Ravindran[1‡], Sriram Kumar[1‡], Johanna Rajkumar[1], Sujata Roy[1], Sekar Sathiya[2], Chidambaram Saravana Babu[2] and Mohammad Javed Equbal[3*]

[1]Department of Biotechnology, Rajalakshmi Engineering College, Chennai−602105, Tamil Nadu, India

[2]Centre for Toxicology and Developmental Research, Sri Ramachandra University, Chennai−600116, Tamil Nadu, India

[3]Biomedical Institute for Regenerative Research, Texas A&M University− Commerce, Commerce−75428, TX, United States

*Corresponding author: Mohammad Javed Equbal, Assistant Professor, Biomedical Institute for Regenerative Research (BIRR), Texas A&M University−Commerce, Commerce 75428, TX, United States, Tel: 903-886-3218; Fax: 903-886-5988; E-mail: Javed.Equbal@tamuc.edu

‡These authors have contributed equally for this study

Abstract

Aims and objectives: The current study characterized the morphology of Ambrex formulation by Scanning Electron Microscopy and assessed its cardioprotective activity against Isoproterenol (ISPH)-induced myocardial necrosis in rats by biochemical and histopathological evaluations, and also attempted to predict the prospective protein-targets of Ambrex and the signaling pathway that mediates this activity through molecular docking approach.

Materials and methods: Sprague–Dawley male rats (4 groups, 6 rats per group) chosen for the current study were acclimatized to the laboratory conditions for 7 days prior to actual treatment; they were pretreated with Ambrex (40 mg/kg b.wt/day, p.o) everday for 21 days and then intoxicated with ISPH (85 mg/kg b.wt, s.c) on day-20 and 21 to experimentally induce myocardial necrosis. The extent of ISPH-induced myocardial necrosis was quantified in terms of the serum levels of two cardiac biomarkers: creatine kinase-MB and lactate dehydrogenase. The extent of ISPH-induced oxidative stress was quantified in terms of the tissue levels of five oxidative stress biomarkers: superoxide dismutase, catalase, reduced glutathione, glutathione peroxidase and lipid peroxidation.

Results and discussion: The Scanning Electron Microscopy image of Ambrex formulation showed the formation of nanoparticles with thickness of 65 nm, making Ambrex a unique metal-deficient Siddha-medicine based polyherbal nano-formulation characterized and evaluated in India. Pretreatment with Ambrex attenuated the extent of ISPH-induced oxidative stress, lipid peroxidation and generation of reactive oxygen species as reflected by biochemical evaluations, and also ameliorated the degree of ISPH-induced myocardial necrosis and membrane damage as reflected by histopathological evaluations. The results of molecular docking revealed that Withaferin-A and Methyl Commate-A (the key metabolites of *Withania somnifera* and Ambrex respectively) inhibit Protein Kinase-C Beta, and renders Ambrex its cardioprotective activity by maintaining the intracellular antioxidant homeostasis and myocardial membrane architecture.

Keywords: Myocardial necrosis; Cardioprotective activity; Siddha medicine; Polyherbal formulation; Oxidative stress; *Withania somnifera*; Withaferin-A; Methyl Commate-A; Protein Kinase-C Beta (PKCβ); Antioxidant homeostasis; Scanning electron microscopy

Abbreviations:

MI: Myocardial Infarction; FTIR: Fourier-Transform Infrared Spectroscopy; GC-MS: Gas Chromatography-Mass Spectrometry; TCA: Tricarboxylic Acid; ICDH: Isocitrate Dehydrogenase; SDH: Succinate Dehydrogenase; α-KGDH: Alpha-Ketoglutarate Dehydrogenase; ISPH: Isoproterenol; SEM: Scanning Electron Microscopy; LDH: Lactate Dehydrogenase; CK-MB Creatine-Kinase MB; SOD: Superoxide Dismutase; CAT: Catalase; GSH: Reduced Glutathione; GPX: Glutathione Peroxidase; LPO: Lipid Peroxidation; H&E: Hematoxylin and Eosin; ANOVA: Analysis of Variance; PKCβ: Protein Kinase-C Beta; PDB: Protein Data Bank; HBAT: Hydrogen Bond Analysis Tool; MNC: Mononuclear Cells; SI: Supplementary Information; GR: Glutathione Reductase; GS: Glutathione Synthase; P: Phosphate; Pin1: Peptidyl-prolyl cis-trans Isomerase NIMA-interacting 1; PP2A: Protein Phosphatase-2A; TIM: Translocase of the Inner Membrane; TOM: Translocase of the Outer Membrane; Cyt.C: Cytochrome-C; H_2O_2: Hydrogen Peroxide; OS: Oxidative Stress; PTP: Permeability Transition Pore; ROS: Reactive Oxygen Species; Rac1: Ras-related C_3 botulinum-toxin substrate-1; FOXO: Forkhead Box-O_3

Introduction

Myocardial Infarction (MI) continues to be the predominant reason of mortality worldwide, in-spite of the steadfast advancements made towards diagnosis and treatment of coronary artery diseases [1]. It is caused by the metabolic imbalance involving elevated energy requirements and deficient oxygen supply to the cardiac myocytes, ultimately leading to myocardial necrosis [2]. MI is closely associated with several changes in metabolic and signaling pathways that involve increased oxidative stress, elevated lipid peroxidation, excessive cytoplasmic/mitochondrial calcification, disturbed antioxidant homeostasis, dynamic cellular metabolism, irreversible DNA damage and other pathophysiological alterations [3]. The mechanism of

pharmacological action exhibited by modern western medicines revolves around the lock-and-key model that entails the action of a single therapeutic agent against a single target to regulate a particular metabolic/signaling pathway, thereby failing to treat diseases governed by multiple molecular mechanisms [4]. The undesirable side-effects linked with the use of these synthetic drugs are also a raising health concern [5].

The Indian traditional system of medicine employs multiple natural ingredients that constitute several active metabolites, thereby imparting a holistic pharmacological activity on multiple targets orchestrating several pathways, without inducing significant side-effects [6]. Ambrex, a licensed polyherbal formulation consists of five 'Generally-Safe' Indian herbs: *Withania somnifera, Cycas circirnalis,* Shorea, robusta, *Orchis mascula* and amber (a resin from *Pinus succinifera*) that are blended together in accordance to the Siddha-system of medicine. In our previous study, FTIR characterization of Ambrex demonstrated C=O stretching in carbonyl compounds contributed by high content of terpenoids and flavanoids [7], while its GC-MS analysis revealed Methyl-Commate-A as the key metabolite in its volatile-fraction [8]. Our previous *in-vivo* study revealed that pretreatment with Ambrex decreases the ISPH-induced up-regulation of apoptotic genes (p53, bax and caspase-3) to their normal levels and increases the ISPH-stimulated down-regulation of TCA-cycle enzymes (ICDH, SDH and α-KGDH) and anti-apoptotic gene (bcl-2) to their normal levels [7].

Our previous *in-vivo* study also revealed that pretreatment with Ambrex renews the ISPH-induced reduction in the serum levels of low-density lipoprotein cholesterol and restores the ISPH-stimulated elevation in the levels of high density lipoprotein cholesterol [9]. Ambrex also exhibits appreciable anti-ulcerogenic, anti-hyperlipidemic, broncho-protective and hepato-protective activities as demonstrated *in-vitro* and *in-vivo* in our previous studies [9-17]. The current study characterized the morphology of Ambrex formulation by SEM and assessed its cardioprotective potential against ISPH-induced myocardial necrosis in rats, in terms of its activity over cardiac biomarkers and antioxidant enzymes through biochemical and histopathological evaluations. The current study also attempted to predict the prospective protein-targets of Ambrex, and the associated metabolic reactions and signaling pathways by molecular docking approach. The results of *in-vivo* and *in-silico* studies were finally correlated to holistically predict the molecular mechanisms governing the cardioprotective activity of Ambrex against ISPH-induced myocardial necrosis in rats.

Materials and Methods

Chemicals, drugs and reagents

Ambrex was procured from Care & Cure Herbs Limited, India and ISPH was procured from Sigma Aldrich, USA. LDH (Lactate Dehydrogenase; Cat ID: BEIS43-LDH) and CK-MB (Creatine-Kinase MB; Cat ID: BEIS04-CK-MB) biochemical assay kits were procured from Spinreact, Spain. Unless mentioned, all the other chemicals, drugs and reagents were of analytical grade and were procured from Himedia, India and Sisco Research Laboratories, India.

Characterization of ambrex

Ambrex was characterized by Scanning Electron Microscopy (SEM) under a 25 KV tungsten-filament based, diffusion-pumped Hitachi SEM S2400. A thin film of the sample was mounted onto the ion sputter coater with gold target grid and was dried under a mercury lamp for 10 min. The images were later captured from 5X to 300,000X magnifications using EDS software.

Experimental animals

Sprague–Dawley male rats weighing 150-200 g b.wt were chosen for the study. A total of twenty four rats were housed in eight solid-bottom hygienic polypropylene cages (3 rats/cage) in a well-ventilated room (15 air cycles/min, 70:30 recycle ratio), under an ambient temperature of 23 ± 2°C, a relative humidity of 40–65% and an artificial photoperiod of 12 hrs light/12 hrs dark cycle (lighted between 7:00–19:00 hrs). They were acclimatized to the laboratory conditions for 7 days prior to treatment and were fed with commercial rodent feed (supplied by Provimi Animal Nutrition India Private Limited, India) and purified water *ad libitum.*

Ethical compliance

The study was reviewed and approved by the Institutional Animal Ethical Committee (IAEC) of Biomedical Research Unit and Laboratory Animal Centre (BRULAC), Saveetha University, India (IAEC Ref. ID: Biotech.REC.002/10). All experiments were strictly executed in accordance with the 'Guide for the Care and Use of Laboratory Animals' framed by the Institute of Laboratory Animal Resources, USA (National Academic Press, NIH publication #85-23, Revised in 1996).

Treatment regimen

The animals were randomized into four groups (6 rats/group). Groups I and II were administered with saline (0.5% carboxymethyl cellulose, 10 ml/kg b.wt/day, p.o) and groups III and IV were administered with Ambrex (40 mg/kg b.wt/day, p.o; dose was fixed based on our previous studies [7-14]) for 21 days. Groups II and IV were subcutaneously injected with ISPH (85 mg/kg b.wt.; dose was fixed based on our previous studies [7-9]) on day-20 and -21 to induce myocardial necrosis. Post treatment, blood was collected from the overnight fasted rats through retro-orbital puncture and was immediately processed for further biochemical evaluations. The animals were then euthanized by briefly exposing to CO_2 gas and the required organs (heart, liver and kidney) were rapidly dissected and processed for further biochemical evaluations and histopathological examinations.

Quantification of cardiac biomarkers

Whole blood was collected from the right carotids of the overnight fasted rats (with simultaneous monitoring of the hemodynamic parameters) in commercially heparinized red-top tubes. It was clotted by leaving it undisturbed for 2 hrs at room temperature and was then centrifuged at 1000-2000xg for 10 min at 4°C. The clot-free supernatants containing serum were quantified for the levels of the two cardiac biomarkers: CK-MB and LDH, by adopting the standard protocols described in CK-MB and LDH biochemical assay kits [18,19] and their levels were expressed in units/L. Absorbance was detected at

their respective wavelength using Rapid Diagnostics Star 21 Plus Semiautomatic Biochemistry Analyzer.

Quantification of oxidative stress markers

The hearts were rapidly dissected from the euthanized rats and were thoroughly washed with ice-cold physiological saline. They were used to prepare 10% homogenates in phosphate buffer (50 mM, pH 7.4) using a tissue homogenizer and the homogenates were centrifuged at 2500 rpm for 10 min at 4°C. The precipitate-free supernatants were quantified for the total protein content by Lowry's method and then for the levels of the five oxidative stress markers: Superoxide Dismutase (SOD), Reduced Glutathione (GSH), Glutathione Peroxidase (GPX), Catalase (CAT) and Lipid Peroxidation (LPO) by adopting the standard protocols [20-24]. Absorbance was detected at their respective wavelengths using ThermoFisher Scientific Multiscan UV Spectrophotometer.

Histopathological examination

The required organs (hearts, livers and kidneys) were rapidly dissected from the euthanized rats and were thoroughly washed with ice-cold physiological saline. Tissue samples were rapidly excised from these organs and were immediately fixed, dehydrated and embedded by adopting the standard protocols. They were then serially sectioned to 5 μm thickness using microtomy, stained with Hematoxylin and Eosin (H&E) stain and were fixed on microscopic slides using DPX mountant. The slides were then examined under a Motic DMB1 2MP light microscope (China) at 40X magnification for treatment-induced structural alterations and the photomicrographs were snapped.

Statistical analysis

The results of the biochemical assays associated with the six animals of each group were expressed as mean ± standard error of the mean (SEM). One-way Analysis of Variance (ANOVA) was applied for the statistical analysis, followed by Tukey's multiple comparison for post-hoc analysis. Statistical analyses were performed using GraphPad prism 5.0 (San Diego, USA) and a p-value<0.05 was considered to be statistically significant.

Molecular docking

A computer system with 4 GB RAM and 450 GB hard disk was used for the *in-silico* analysis. The crystal structures of the target-protein PKCβ (PDB ID: 2I0E) and all the test-ligands were procured from Protein Data Bank and PubChem respectively [25-27] and were processed using Python scripts of Autodock tools. The test-ligands were separately docked at the ligand-binding sites of the corresponding target-proteins using Autodock Vina 4.5 [28]. The docked structures were visualized in BIOVIA Discovery Studio Visualizer 2016 [29] and the associated interaction energies were tabulated. Binding of a particular test-ligand with a target-protein was regarded to be favorable, if its interaction energy was lesser than that of the corresponding control-ligand. The H-bonds formed between the target-proteins and corresponding test-ligands were analyzed using HBAT 1.1 software [30] and the interactions were visualized in PyMol Molecular Graphics Viewer v4.3.0 [31]. H-bonds involving electronegative atoms (like O, N, S etc.) were considered to be strong and those involving Carbon as donor atoms were considered to be weak [32-35].

Results

Characterization of ambrex

SEM serves as an effective tool for the morphological characterization of nanoparticle-based herbal medicines. The SEM image of Ambrex formulation (Figure 1) showed the formation of rough, discrete and highly porous nanoparticles with thickness as low as 65 nm. The image also showed the absence of any aggregates, revealing the complete blending of different constituents of Ambrex.
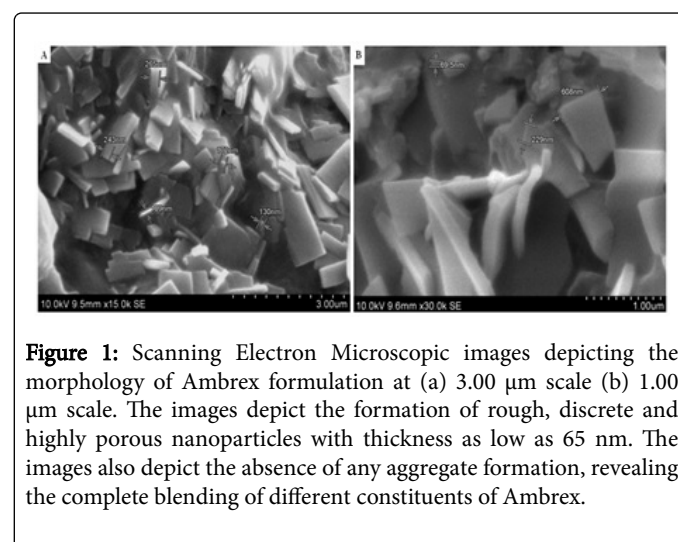

Figure 1: Scanning Electron Microscopic images depicting the morphology of Ambrex formulation at (a) 3.00 μm scale (b) 1.00 μm scale. The images depict the formation of rough, discrete and highly porous nanoparticles with thickness as low as 65 nm. The images also depict the absence of any aggregate formation, revealing the complete blending of different constituents of Ambrex.

Quantification of cardiac biomarkers

The serum levels of the two cardiac markers: CK-MB and LDH in the four groups of study rats are consolidated in Table 1. ISPH-treated group-II rats had significant increase in CKMB [$F_{(3,20)}$=163.10, p ≤ 0.01] and LDH ($F_{(3,20)}$=49.15, p ≤ 0.01) levels when compared with untreated group-I control rats. Ambrex-pretreated and ISPH-treated group-IV rats had significant decrease in CK-MB [p ≤ 0.01] and LDH [p ≤ 0.01] levels when compared with ISPH-treated group-II rats. The serum levels of these two cardiac biomarkers in Ambrex-pretreated group-III rats had no significant change when compared with untreated group-I control rats.

Cardiac Biomarkers	Group-I: Normal Control	Group-II: ISPH (85 mg/kg)	Group-III: Ambrex (40 mg/kg)	Group-IV: Ambrex + ISPH
CK-MB (Units/L)	179.2 ± 5.9	375.2 ± 5.94**	195.05 ± 8.4	207.4 ± 8.01##

LDH (Units/L)	196.82 ± 7.26	331.7 ± 7.7**	218.63 ± 9.09	219.0 ± 10.4##

Note: Values are expressed as mean ± SEM where n=6/group. Significance with Tukey's test following one-way ANOVA are indicated as: **p ≤ 0.01 when compared with group-I (normal control); ##p ≤ 0.01 when compared with group-II (ISPH treated). CK-MB: Creatine-Kinase MB; LDH: Lactate Dehydrogenase; ISPH: Isoproterenol

Table 1: Biochemical Quantification of Cardiac Biomarkers.

Quantification of oxidative stress markers

The tissue levels of the five oxidative stress markers: SOD, CAT, GSH, GPX and LPO in the four groups of study rats are listed in Table 2. ISPH-treated group-II rats had significant decrease in SOD $[F_{(3,20)}=22.06, p \leq 0.01]$, CAT $[F_{(3,20)}=8.47, p \leq 0.01]$, GSH $[F_{(3,20)}=9.52, p \leq 0.01]$, GPX $[F_{(3,20)}=6.67, p \leq 0.01]$ and LPO $[F_{(3,20)}=64.97 p \leq 0.01]$ levels when compared with untreated group-I control rats. Ambrex-pretreated and ISPH-treated group-IV rats had significant increase in SOD [p ≤ 0.01], CAT [p ≤ 0.05], GSH [p ≤ 0.05], GPX [p ≤ 0.05] and LPO [p ≤ 0.01] levels when compared with ISPH-treated group-II rats. The tissue levels of these five oxidative stress markers in Ambrex-pretreated group-III rats had no significant change than untreated group-I control rats.

Oxidative Stress Markers	Group-I: Normal Control	Group-II: ISPH (85 mg/kg)	Group-III: Ambrex (40 mg/kg)	Group-IV: Ambrex + ISPH
SOD (Units/mg protein)	375.43 ± 7.52	273.19 ± 10.57**	352.74 ± 11.3	343.15 ± 7.52##
CAT (µmol/mg protein)	9.91 ± 0.80	6.78 ± 0.44**	9.41 ± 0.13	8.90 ± 0.21#
GSH (µmol/mg protein)	6.71 ± 0.60	4.09 ± 0.25**	6.01 ± 0.2	5.81 ± 0.24#
GPx (µmol/mg protein)	0.44 ± 0.01	0.32 ± 0.02**	0.43 ± 0.03	0.41 ± 0.02#
LPO (µmol/mg protein)	61.12 ± 0.09	81.24 ± 0.03**	61.23 ± 0.13	61.16 ± 0.19##

Note: Values are expressed as mean ± SEM where n=6/group. Significance with Tukey's test following one-way ANOVA are indicated as: **p ≤ 0.01 whsen compared with group-I (normal control); #p ≤ 0.05 and ##p ≤ 0.01when compared with group-II (ISPH treated). ISPH: Isoproterenol; SOD: Superoxide Dismutase; CAT: Catalase; GSH: Reduced Glutathione; GPX: Glutathione Peroxidase; LPO: Lipid Peroxidation

Table 2: Biochemical quantification of oxidative stress markers.

Histopathological examination

Histopathological examination of the myocardial tissues collected from ISPH-treated group-II rats showed an irreversible cardiac injury (characterized by extensive foci of myocardial necrosis and interstitial fibrosis) (Figure 2a). It was also associated with mild to severe multifocal myocardial degeneration (characterized by extensive sarcoplasmic swelling and hyper-eosinophilia of cardiac myocytes), in addition to marked interstitial infiltration of mononuclear cells (MNCs). In contract, histopathological examination of the myocardial tissues collected from Ambrex-pretreated and ISPH-treated group-IV rats showed a reversible cardiac injury (characterized by mild interstitial edema), in association with minimal to moderate myocardial degeneration (characterized by mild sarcoplasmic alterations and minimal interstitial infiltration of mononuclear cells) (Figure 2b). Histopathological examination of the myocardial tissues collected from Ambrex-pretreated group-III rats (Figure 2c) showed no treatment-induced histoarchitectural or pathophysiological alterations when compared with myocardial tissues collected from untreated group-I control rats (Figure 2d).
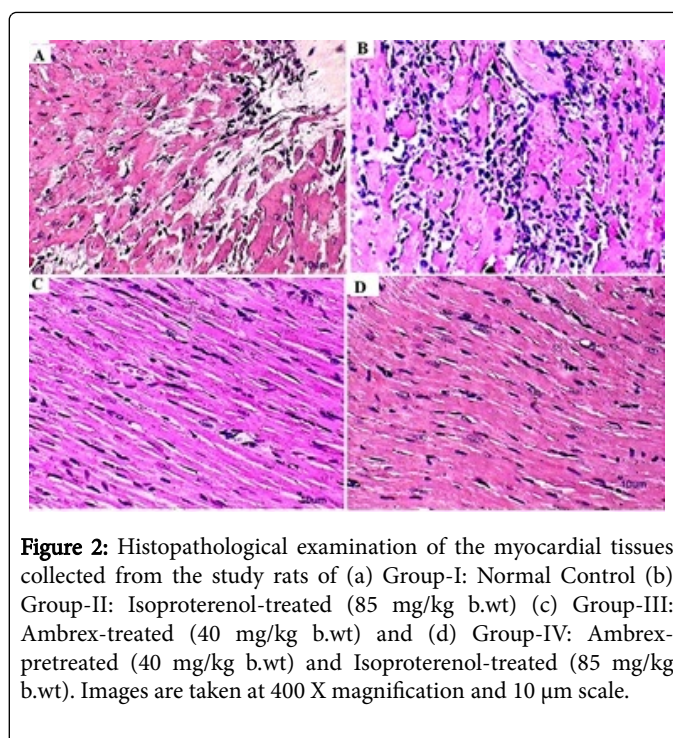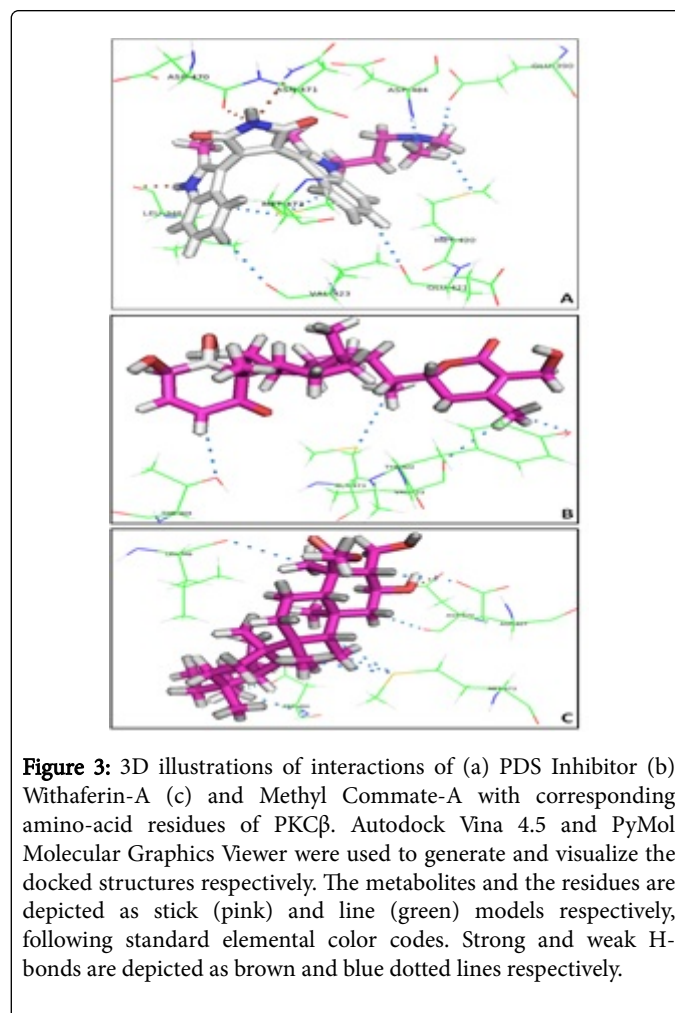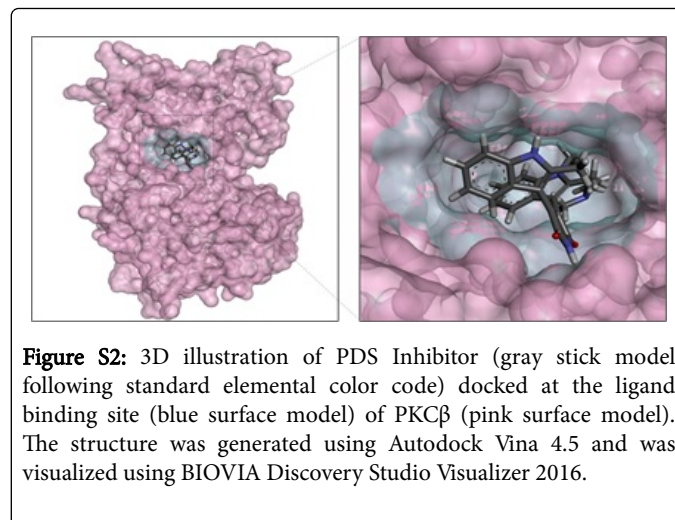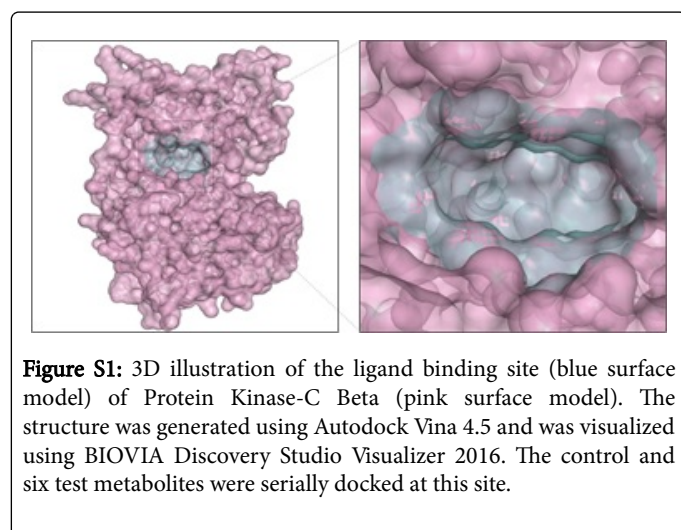

Figure 2: Histopathological examination of the myocardial tissues collected from the study rats of (a) Group-I: Normal Control (b) Group-II: Isoproterenol-treated (85 mg/kg b.wt) (c) Group-III: Ambrex-treated (40 mg/kg b.wt) and (d) Group-IV: Ambrex-pretreated (40 mg/kg b.wt) and Isoproterenol-treated (85 mg/kg b.wt). Images are taken at 400 X magnification and 10 µm scale.

Molecular docking

The interaction energies of PDS Inhibitor, Withaferin-A and Methyl Commate-A with PKCβ were -7.0 Kcal/mol, -8.9 Kcal/mol and -8.0 Kcal/mol respectively (Table 3), indicating that the interactions of Withaferin-A and Methyl Commate-A with PKCβ are better than that of PDS Inhibitor. The structure of PDS Inhibitor docked with PKCβ at its binding site (Supplementary Information (SI) Figures S1 and S2) illustrated that it interacts with Met-473, Val-423, Glu-421, Asp-484, Met-420 and Glu-390 residues of the protein through weak H-bonds and with Leu-348, Asp-470 and Asp-471 residues through strong H-bonds (Figure 3a). The structure of Withaferin-A docked with PKCβ at PDS Inhibitor binding site (Figure S3) illustrated that it interacts with Thr-404, Val-423, Tyr-422 and Met-473 residues of the protein through weak H-bonds (Figure 3b). The structure of Methyl Commate-A docked with PKCβ at PDS Inhibitor binding site (Figure S4) illustrated that it interacts with Asp-427, Met-473, Asp-470, Leu-348 and Asp-484 residues of the protein through weak H-bonds and with Asp-470 residue through strong H-bond (Figure 3c). The structures of the other metabolites docked with PKCβ at PDS Inhibitor binding site are illustrated in Figures S5-S8, and their interactions with the amino-acid residues of PKCβ are illustrated in Figure S9a-S9d. The list of H-bonds formed by the seven metabolites with the amino-acid residues of PKCβ is consolidated in Table S1.

Interacting Metabolites	Source Herbs of the Metabolites	Interaction Energies with PKCβ (Kcal/mol)
PDS Inhibitor	-	-7.0
Withaferin-A	*Withania somnifera*	-8.9
Stearic Acid	*Shorea robusta*	-5.9
Glucomannan	*Orchis mascula*	-7.4
Trehalose	*Cycas circirnalis*	-7.0
Succinic-Acid	*Pinus succinifera*	-4.3
Methyl-Commate-A	Ambrex Formulation	-8.0

Table 3: Interaction energies of key metabolites of Ambrex docked with PKCβ.

Figure S1: 3D illustration of the ligand binding site (blue surface model) of Protein Kinase-C Beta (pink surface model). The structure was generated using Autodock Vina 4.5 and was visualized using BIOVIA Discovery Studio Visualizer 2016. The control and six test metabolites were serially docked at this site.

Figure S2: 3D illustration of PDS Inhibitor (gray stick model following standard elemental color code) docked at the ligand binding site (blue surface model) of PKCβ (pink surface model). The structure was generated using Autodock Vina 4.5 and was visualized using BIOVIA Discovery Studio Visualizer 2016.

Figure 3: 3D illustrations of interactions of (a) PDS Inhibitor (b) Withaferin-A (c) and Methyl Commate-A with corresponding amino-acid residues of PKCβ. Autodock Vina 4.5 and PyMol Molecular Graphics Viewer were used to generate and visualize the docked structures respectively. The metabolites and the residues are depicted as stick (pink) and line (green) models respectively, following standard elemental color codes. Strong and weak H-bonds are depicted as brown and blue dotted lines respectively.
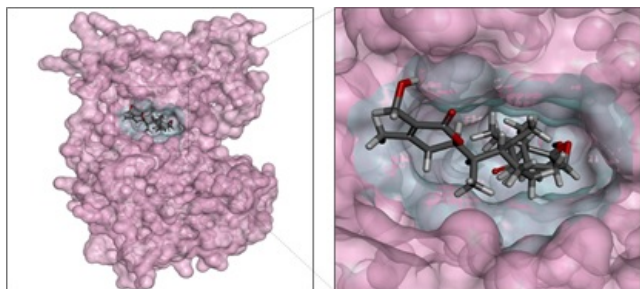
Figure S3: 3D illustration of Withaferin-A (gray stick model following standard elemental color code) docked at the ligand binding site (blue surface model) of PKCβ (pink surface model). The structure was generated using Autodock Vina 4.5 and was visualized using BIOVIA Discovery Studio Visualizer 2016.
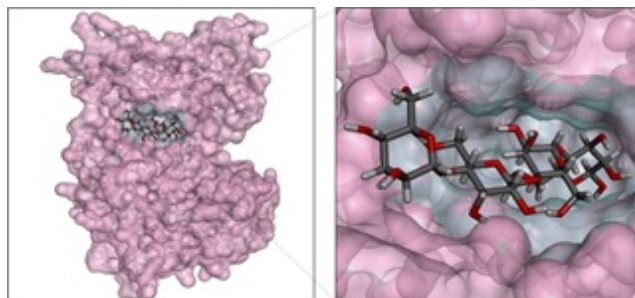

Figure S6: 3D illustration of Glucomannan (gray stick model following standard elemental color code) docked at the ligand binding site (blue surface model) of PKCβ (pink surface model). The structure was generated using Autodock Vina 4.5 and was visualized using BIOVIA Discovery Studio Visualizer 2016.

Figure S4: 3D illustration of Methyl Commate-A (gray stick model with standard elemental color code) docked at the ligand binding site (blue surface model) of PKCβ (pink surface model). The structure was generated using Autodock Vina 4.5 and was visualized using BIOVIA Discovery Studio Visualizer 2016.
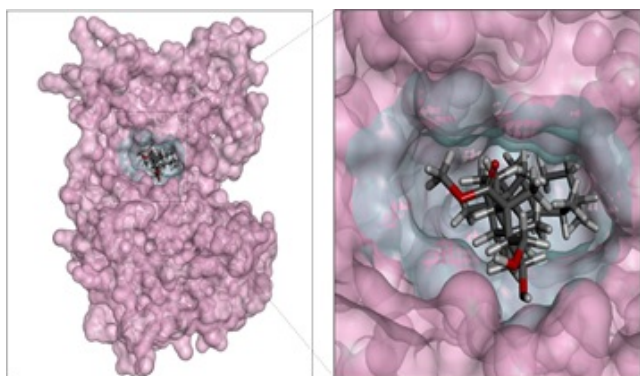

Figure S7: 3D illustration of Trehalose (the gray stick model following standard elemental color code) docked at the ligand binding site (blue surface model) of PKCβ (pink surface model). The structure was generated using Autodock Vina 4.5 and was visualized using BIOVIA Discovery Studio Visualizer 2016.
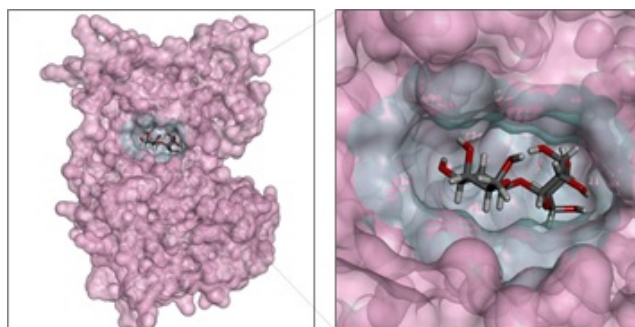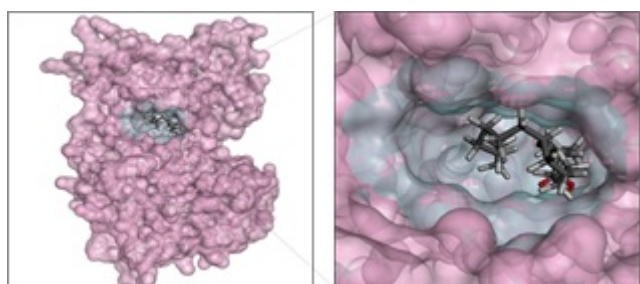

Figure S5: 3D illustration of Stearic Acid (gray stick model following standard elemental color code) docked at the ligand binding site (blue surface model) of PKCβ (pink surface model). The structure was generated using Autodock Vina 4.5 and was visualized using BIOVIA Discovery Studio Visualizer 2016.

Figure S8: 3D illustration of Succinic Acid (gray stick model following standard elemental color code) docked at the ligand binding site (blue surface model) of PKCβ (pink surface model). The structure was generated using Autodock Vina 4.5 and was visualized using BIOVIA Discovery Studio Visualizer 2016.
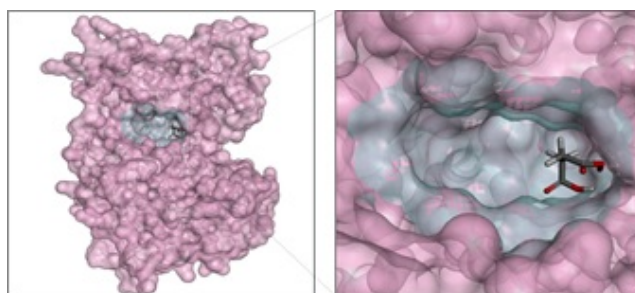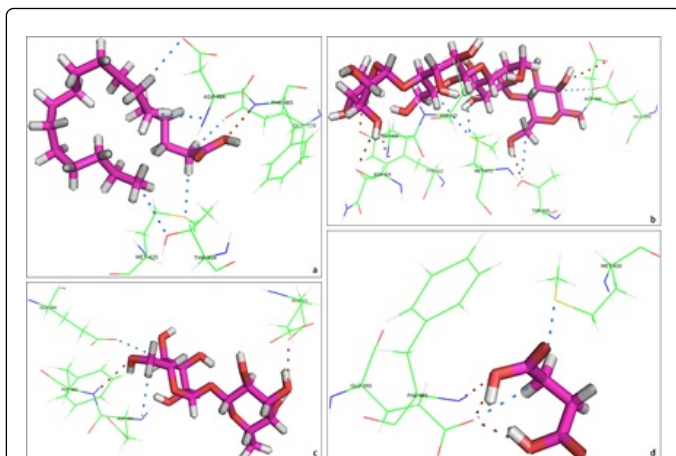
Figure S9: 3D illustrations of interactions of (a) Stearic Acid (b) Glucomannan (c) Trehalose and (d) Succinic-acid with corresponding amino-acid residues of PKCβ. Autodock Vina 4.5 and PyMol Molecular Graphics Viewer were used to generate and visualize the docked structures respectively. The metabolites and the residues are represented in stick (pink) and line (green) models respectively, following standard elemental color codes. Strong and weak H-bonds are depicted as brown and blue dotted lines, respectively.

Atoms from the Test Metabolites	Atoms from the Target-Protein	Length of Bonds (Å)
PDS Inhibitor docked with Protein Kinase-C Beta		
C5	MET473:SD	3.4
C6	VAL423:O	3.9
N10	LEU348:O	3.2
N15	ASP470:O	2.8
N15	ASN471:ND2	3.4
C23	GLU421:O	3.6
C25	MET473:SD	3.8
C31	ASP484:N	3.4
C32	MET420:SD	3.6
C32	GLU390:OE1	3.2
Withaferin-A docked with Protein Kinase-C Beta		
C26	THR404: OG1	3.6
C1	VAL423:O	3.8
C1	TYR422:OH	3.5
C10	MET473:SD	3.9
Stearic Acid docked with Protein Kinase-C Beta		
C1	TYR404: OG1	3.6
C12	ASP484: OD1	3.8
C13	ASP484: N	3.6
C17	MET420: SD	3.7
C17	GLU390: OE1	3.4
O20	PHE485: N	3
Trehalose docked with Protein Kinase-C Beta		
O21	GLU421: O	3
C12	GLU390:OE1	3.6
C15	ASP484:N	3.4
O16	PHE485:N	3.1
Glucomannan docked with Protein Kinase-C Beta		
C10	MET473:SD	3.9
C14	ASP427:OD2	3.2
C12	MET473:SD	3.8
O43	ASN424:O	3.1
O43	GLY426:N	3.3
O45	TYR422:OH	2.9
C31	GLU390:OE1	3.5
O34	ASP484:OD2	3.5
C36	THR404:OG1	3.4
O37	THR404:OG1	2.9
Succinic Acid docked with Protein Kinase-C Beta		
C2	GLU390:OE1	3.4
C2	MET420:SD	3.9
O5	GLU390:OE1	2.9
O5	PHE485:N	3
O8	GLU390:OE1	2.8
Methyl Commate-A docked with Protein Kinase-C Beta		
C5	ASP427:OD2	3.5
C21	MET473:SD	3.7
C9	ASP470:O	3.5
C23	MET473:SD	3.6
C13	LEU348:O	3.7
O10	ASP470:OD2	3.2
C42	MET473:SD	3.4
C38	ASP484:OD2	3.8
C38	ASP484:N	3.7

Table S1: List of H-bonds formed by the test metabolites with the amino-acid residues of PKCβ.

Discussion

The current study characterized the morphology of Ambrex formulation by SEM, assessed its cardioprotective potential against ISPH-induced myocardial necrosis in rats through biochemical and histopathological evaluations, and predicted the prospective signaling pathway that mediates this activity through molecular docking approach. The particle-size of Ambrex in the nano-range as illustrated by SEM-characterization could be conferred by the unique method of nano-grinding adopted for its formulation. This morphological characteristic of Ambrex enhances its *in-vivo* pharmacological action through numerous mechanisms, like quicker dissolution due to increased surface area, enhanced permeation through membrane barriers due to small size, longer retention in target tissues due to reduced lymphatic drainage, enhanced bioavailability due to higher loading capacities, reduced hepatic and renal toxicities due to targeted delivery, enhanced stability without additional ligand moieties [36]. To the best of our knowledge, Ambrex is a unique metal-deficient Siddha-medicine based polyherbal nano-formulation characterized and evaluated in India.

Deficient supply of oxygen/glucose and/or excessive accumulation of calcium in the myocardial cytosol disrupt the integrity and permeability of the myocardial membrane, causing a leakage of the cardiac biomarker enzymes like CK-MB and LDH from the cytosol into the extracellular fluid [37]. Moreover, the amount of these enzymes released into the serum is closely associated with the number of necrotic cells and extent of necrosis in response to -adrenergic stimulation, as these enzymes are comparatively abundant in the myocardial tissues and are apparently absent in most other tissues [38]. In the present study, treatment with ISPH significantly elevated the serum levels of these two enzymes in the group-II rats when compared with their respective normal levels in group-I rats. Nonetheless, pretreatment with Ambrex significantly maintained the serum levels of these two enzymes at their respective normal levels in the group-IV rats. These outcomes suggest that Ambrex confers cardioprotectivity by maintaining the integrity and permeability of the myocardial membrane, thereby preventing the leakage of these enzymes into the serum.

The quinine metabolites produced through ISPH-oxidation react with oxygen to form superoxides and other free-radicals, which further perturb the intracellular antioxidant homeostasis [39]. The endogenous antioxidant enzymes are highly instrumental for the neutralization of free-radical-mediated oxidative stress [40]. SOD, CAT and GPX are the primary hydroxyl-radical scavenging antioxidant enzymes that decompose O_2 and H_2O_2, prior to their fusion to form highly-reactive hydroxyl-radicals [41]. In the current study, treatment with ISPH significantly reduced the tissue levels of these enzymes in the group-II rats when compared with their respective normal levels in group-I rats. The reduced levels of these enzymes can be attributed to their increased uptake for neutralizing the free-radicals and/or their reduced expression due to excessive ISPH-oxidation [42]. Pretreatment with Ambrex significantly maintained the tissue levels of these 5 enzymes at their respective normal levels in group-IV rats. These results imply that Ambrex imparts cardioprotectivity by maintaining the expression levels of these enzymes such that their cytoplasmic reserves will equalize to normal, despite the utilization and degradation of a fraction of these enzymes for scavenging the free-radicals.

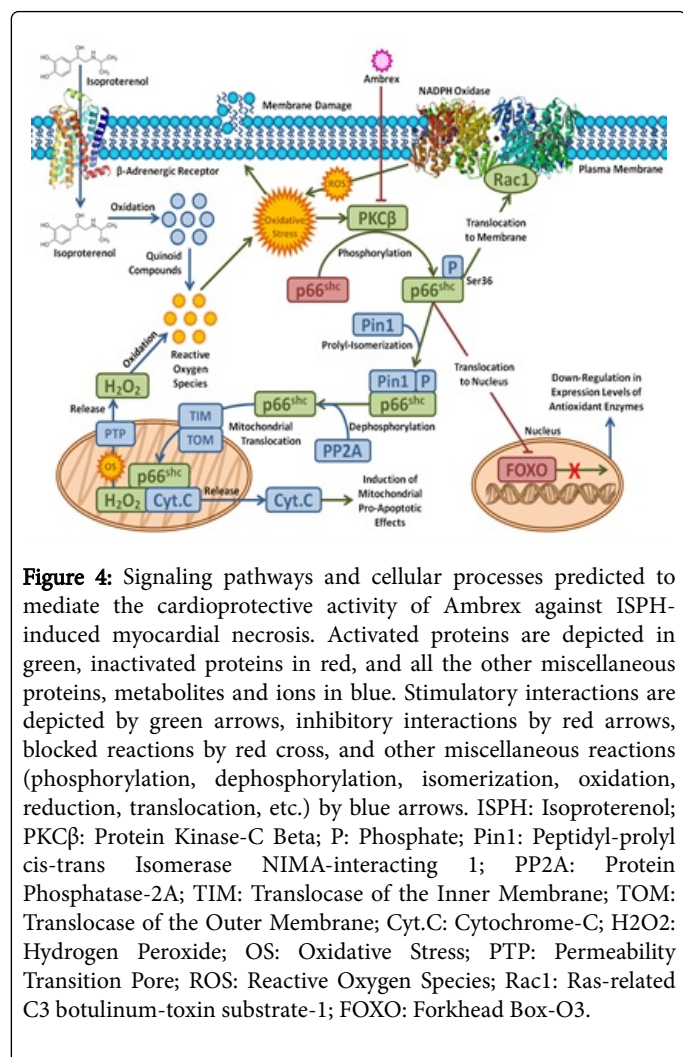LPO serves as an effective indicator of ISPH-induced myocardial necrosis and is closely associated with compromised myocardial membrane and disturbed antioxidant machinery [43]. Higher rates of LPO contribute to higher levels of malondialdehyde (a major end-product of LPO) that elevates the levels of free-radicals, ultimately disrupting the myocardial membrane and/or inactivating the antioxidant enzymes [44]. In the present study, treatment with ISPH significantly elevated the tissue LPO level in the group-II rats when compared with its normal level in group-I rats. The elevation in LPO levels can be considered as the preliminary phase in the pathogenesis of ISPH-induced myocardial necrosis, which later induces free-radical mediated oxidative stress and disrupts the membrane integrity and permeability [44]. However, pretreatment with Ambrex significantly maintained the tissue LPO level at normal in the group-IV rats. These outcomes suggest that constituents of Ambrex may possess free-radical scavenging activity and neutralize the free-radicals produced by excessive LPO, thereby rendering Ambrex its effective cardioprotective potential.

GSH is an endogenous non-enzymatic antioxidant biomolecule present in the cells that coordinates with the enzymatic antioxidant system involving SOD, CAT, GPX and Glutathione Reductase (GR) to effectively scavenge the free-radicals such as peroxides, superoxides and alkoxy-radicals [45]. Serving as the substrate for two antioxidant enzymes GPX and Glutathione Synthase (GS), it protects the cells from the cytotoxic effects of peroxides and superoxides generated by the oxidation of ISPH [46]. In the current study, treatment with ISPH significantly reduced the tissue level of this biomolecule in the group-II rats when compared with its respective normal level in group-I rats. The reduced level of this biomolecule can be associated with its increased utilization for orchestrating the activities of GS and GPX. Nonetheless, pretreatment with Ambrex significantly maintains the tissue level of this biomolecule at its normal level in the group-IV rats. These results indicate that Ambrex demonstrates cardioprotective potential by maintaining the synthesizing-activity of GS and/or the reducing-activity of GR, thereby maintaining the rates of GSH synthesis.

Cardioprotective phytocompounds and synthetic drugs are known to protect the cardiac myocytes from ISPH-induced oxidative stress by upregulating the expression of antioxidant enzymes and/or by inhibiting the downstream targets of β-adrenergic receptor, thereby reducing the formation of cytotoxic free-radicals [47]. It is reported that oxidative stress activates PKCβ, which further phosphorylates p66Shc, thereby facilitating its translocation from the cytoplasm to the mitochondrion, where phosphorylated p66Shc induces further oxidative stress and amplifies the negative feedback. It is also reported that phosphorylated p66Shc translocates to the nucleus and inhibits FOXO transcription factors, thereby down-regulating the expression of antioxidant enzymes; while it also moves to the plasma membrane and activates NADPH Oxidase through rac1, thereby generating ROS [48]. Hence, the prospect of these signalling proteins as targets for Ambrex was analyzed by docking the key metabolites of its constituent herbs with PKCβ as the target, considering PDS Inhibitor as the control [49-53]. In our previous phytochemical study, GC-MS results revealed Methyl Commate-A as the key metabolite in the volatile-fraction of Ambrex, which was also considered for this docking study [8].

Protein Kinase-C Beta (PKCβ) is a cytoplasmic kinase that regulates the functions of several other downstream protein-targets by phosphorylating site-specific serine and threonine amino-acid residues of these proteins at their hydroxyl groups [48]. The results of molecular docking carried-out in the current study revealed that Withaferin-A and Methyl Commate-A (the key metabolites of *Withania somnifera*

and Ambrex respectively) inhibit PKCβ, and prevent it from phosphorylating p66Shc. Unphosphorylated p66Shc would therefore be checked from translocating to the mitochondrion and plasma-membrane, and hence would be prevented from inducing further oxidative stress and amplifying the negative feedback. It would also be checked from translocating to the nucleus, which would keep the FOXO transcription factors active at their respective normal levels, resulting in the expression and activities of antioxidant enzymes at their respective normal levels (Figure 4). This in-silico prediction pertinently agrees with our biochemical quantification results of oxidative stress markers (Table 2). This suggests that Ambrex exhibits cardioprotectivity by maintaining the intracellular antioxidant homeostasis and myocardial membrane architecture probably through the inhibition of PKCβ.

Figure 4: Signaling pathways and cellular processes predicted to mediate the cardioprotective activity of Ambrex against ISPH-induced myocardial necrosis. Activated proteins are depicted in green, inactivated proteins in red, and all the other miscellaneous proteins, metabolites and ions in blue. Stimulatory interactions are depicted by green arrows, inhibitory interactions by red arrows, blocked reactions by red cross, and other miscellaneous reactions (phosphorylation, dephosphorylation, isomerization, oxidation, reduction, translocation, etc.) by blue arrows. ISPH: Isoproterenol; PKCβ: Protein Kinase-C Beta; P: Phosphate; Pin1: Peptidyl-prolyl cis-trans Isomerase NIMA-interacting 1; PP2A: Protein Phosphatase-2A; TIM: Translocase of the Inner Membrane; TOM: Translocase of the Outer Membrane; Cyt.C: Cytochrome-C; H2O2: Hydrogen Peroxide; OS: Oxidative Stress; PTP: Permeability Transition Pore; ROS: Reactive Oxygen Species; Rac1: Ras-related C3 botulinum-toxin substrate-1; FOXO: Forkhead Box-O3.

The severe histopathological abnormalities observed in the cardiac myocytes procured from ISPH-treated group-II rats could be because of disturbed antioxidant homeostasis and disrupted membrane architecture caused by ISPH-induced oxidative stress, free-radical mediated LPO and excessive intracellular acidification. The moderate morphological modifications observed in the cardiac myocytes procured from Ambrex-pretreated and ISPH-treated group-IV rats could be due to maintained antioxidant homeostasis and preserved membrane architecture, possibly resulted by reduced ISPH-induced

oxidative stress, and hence reduced intracellular acidification and free-radical mediated LPO, probably due to the inhibition of PKCβ by Withaferin-A and Methyl Commate-A of Ambrex. The future scopes of the current study shall include: confirming our *in-silico* predictions through appropriate *in-vitro* and *in-vivo* experiments, screening for the existence of other key metabolites in Ambrex by relevant phytochemical assays, identifying their prospective protein-targets and signalling pathways that govern their respective mechanisms of actions, and undertaking an overall omics-approach to study the regulatory effects of Ambrex on the different cellular components associated with MI.

Conclusion

The current study characterized the morphology of Ambrex formulation by SEM and assessed its cardioprotective activity against ISPH-induced myocardial necrosis in rats, by quantifying its effects on different cardiac biomarkers and oxidative stress markers through biochemical and histopathological evaluations. To the best of our knowledge, Ambrex serves as a unique metal-deficient Siddha-medicine based polyherbal nano-formulation characterized and evaluated in India. Pretreatment with Ambrex significantly maintained the serum levels of cardiac biomarkers and tissue levels of oxidative stress markers at their respective normals. It also attenuated the magnitude of ISPH-induced oxidative stress, ROS generation and LPO as reflected by biochemical evaluations, and ameliorated the degree of ISPH-induced myocardial necrosis and membrane damage as reflected by histopathological evaluations. The current study also attempted to predict the prospective protein-targets of Ambrex and the signaling pathway that mediates this activity through a molecular docking approach, which suggested that Ambrex exhibits cardioprotective activity by maintaining the intracellular antioxidant homeostasis and myocardial membrane architecture probably through the inhibition of PKCβ protein.

Acknowledgements

Conflict of Interest

The authors declare that there is no conflict of interest.

References

1. Boudina S, Laclau MN, Tariosse L, Daret D, Gouverneur G, et al. (2002) Alteration of mitochondrial function in a model of chronic ischemia in-vivo in rat heart. Am J Physiol Heart Circ Physiol 282: H821-831.

2. Mohanty I, Arya DS, Dinda A, Talwar KK, Joshi S, et al. (2004) Mechanisms of cardioprotective effect of withania somnifera in experimentally induced myocardial infarction. Basic Clin Pharmacol Toxicol 94: 184-190.

3. Meier P, Lansky AJ, Baumbach A (2013) Almanac 2013: Acute Coronary Syndromes. Turk Kardiyol Dern Ars 41: 755-764.

4. Liu YT, Zhou C, Jia HM, Chang X, Zou ZM (2016) Standardized chinese formula xin-ke-shu inhibits the myocardium ca2+ overloading and metabolic alternations in isoproterenol induced myocardial infarction rats. Sci Rep 6: 1-15.

5. Flordellis C, Papathanasopoulos P, Lymperopoulos A, Matsoukas J, Paris H (2007) Emerging therapeutic approaches multi-targeting receptor tyrosine kinases and g-protein coupled receptors in cardiovascular disease. Cardiovasc Hematol Agents Med Chem 5: 133-145.

6. Pal SK, Shukla Y (2003) Herbal Medicine: Current Status and the Future. Asian Pac J Cancer Prev 4: 281-288.

7. Ravindran R, Sathiya S, Devi AJ, Babu CS, Rajkumar J (2015) Studies on the effect of ambrex (an amber based herbal formulation) on apoptotic gene expression and energy producing mitochondrial enzymes in isoproterenol induced myocardial infarction in rats. J Pure Appl Microbiol 9: 803-808.

8. Ravindran R, Lavanya P, Devi AJ, Krithika R, Rajkumar J (2014) Phytochemical screening, gc-ms analysis and antimicrobial evaluation of ambrex (a herbal formulation). Journal of Chemical and Pharmaceutical Sciences 2: 31-35.

9. Ravindran R, Lavanya P, Devi AJ, Rajkumar J (2015) Effect of a poly-herbal formulation, ambrex, on serum lipid profile in isoproterenol induced myocardial infarction in rats. Asian J Microbiol Biotechnol Environ Sci 17: 59-62.

10. Narayan S, Devi RS, Jainu M, Sabitha KE, Devi CS (2004) Protective effect of a polyherbal drug, ambrex, in ethanol induced gastric mucosal lesions in experimental rats. Indian J Pharmacol 36: 34-37.

11. Jainu M, Devi CS (2004) Effect of ambrex (an amber based formulation) on gastric mucosal damage: role of antioxidant enzymes and lipid profile. Indian J Physiol Pharmacol 48: 343-347.

12. Devi AJ, Ravindran R, Sankar M, Rajkumar J (2014) Effect of ambrex (a herbal formulation) on oxidative stress in hyperlipidemic rats and differentiation of 3T3-L1 preadipocytes. Pharmacogn Mag 10: 165-171.

13. Devi J, Rajkumar J (2013) Antihyperlipidemic effect of ambrex, a polyherbal formulation, against experimentally induced hypercholesterolemia in rats. Afr J Pharm Pharmacol 7: 1737-1743.

14. Devi J, Rajkumar J (2014) Effect of ambrex (An Herbal Formulation) on hematological variables in hyperlipidemic rats. Pak J Biol Sci 17: 740-743.

15. Devi RS, Narayan S, Mohan KV, Sabitha KE, Devi S (2003) Effect of a polyherbal formulation, ambrex, on butylated hydroxy toluene induced toxicity in rats. Indian J Exp Biol 41: 1294-1299.

16. Raslin A, Sathiya S, Babu CS, Rajkumar J (2015) in-vitro and in-vivo protective effects of ambrex, a polyherbal formulation, against methotrexate induced damages in hepatic cells. Int J Pharm Pharm Sci 7: 164-170.

17. Raslin A, Sathiya S, Babu CS, Rajkumar J (2017) Attenuation of oxidative stress and hepatotoxicity induced by d–galactosamine by a polyherbal formulation ambrex - in-vivo and in-vitro studies. Indian Journal of Pharmaceutical Education and Research 51: 729-739.

18. Young DS (1997) Effects of drugs on clinical laboratory tests. Ann Clin Biochem 34: 579-581.

19. Thomas L (1998) Clinical laboratory diagnostics, use and assessment of clinical laboratory results. (1st Edition), TH-Books, Frankfurt, Germany.

20. Kakkar P, Das B, Viswanathan PN (1984) A Modified Spectrophotometric Assay of Superoxide Dismutase. Indian J Biochem Biophys 21: 130-132.

21. Sinha AK (1972) Colorimetric assay of catalase. Anal Biochem 47: 389-394.

22. Moron MS, Depierre JW, Mannervik B (1979) Levels of Glutathione, Glutathione Reductase and Glutathione-S-Transferase Activities in Rat Lung and Liver. Biochim Biophys Acta 582: 67-78.

23. Rotruck JT, Pope AL, Ganther HE, Swanson AB, Hafeman DG, et al. (1973) Selenium: Biochemical Role as a Component of Glutathione Peroxidase. Science 179: 588-590.

24. Ohkawa H, Ohishi N, Yagi K (1979) Assay for lipid peroxides in animal tissues by thiobarbituric acid reaction. Anal Biochem 95: 351-358.

25. Dolinsky TJ, Nielsen JE, McCammon JA, Baker NA (2004) PDB2PQR: an automated pipeline for the setup of poisson - boltzmann electrostatics calculations. Nucleic Acids Res 32: W665-W667.

26. Sadowski J, Gasteiger J, Klebe G (1994) Comparison of automatic three-dimensional model builders using 639 X-Ray structures. J Chem Inf Comput Sci 34: 1000-1008.

27. Sadowski J, Schwab CH, Gasteiger J (2003) 3D Structure Generator (Version 3.0), Molecular Networks GmbH Computerchemie, Erlangen, Germany.

28. Trott O, Olson AJ (2010) Autodock Vina: improving the speed and accuracy of docking with a new scoring function, efficient optimization, and multithreading. J Comput Chem 31: 455-461.

29. Dassault Systèmes BIOVIA (2017) Discovery studio modeling environment. (release 2017), Accelrys Software Inc., San Diego, USA.

30. Tiwari A, Panigrahi SK (2007) HBAT: A complete package for analysing strong and weak hydrogen bonds in macromolecular crystal structures. In-Silico Biol 7: 651-661.

31. DeLano WL (2002) Pymol: An open-source molecular graphics tool. CCP4 Newsletter on Protein Crystallography 40: 82-92.

32. Rajan S, Baek K, Yoon HS (2013) C-H…O hydrogen bonds in fk506-binding protein - ligand interactions. J Mol Recognit 26: 550-555.

33. Sarkhel S, Desiraju GR (2004) NOH…O, OOH…O, and COH…O hydrogen bonds in protein-ligand complexes: strong and weak interactions in molecular recognition. Proteins 54: 247-259.

34. Horowitz S, Trievel RC (2012) Carbon - Oxygen Hydrogen Bonding in Biological Structure and Function. J Biol Chem 287: 41576-41582.

35. Horowitz S, Dirk LM, Yesselman JD, Nimtz JS, Adhikari U, et al. (2013) Conservation and Functional Importance of Carbon - Oxygen Hydrogen Bonding in Adomet-Dependent Methyltransferases. J Am Chem Soc 135: 15536-15548.

36. Ansari SH, Islam F, Sameem M (2012) Influence of Nanotechnology on Herbal Drugs: A Review. J Adv Pharm Technol Res 3: 142-146.

37. Priscilla DH, Prince PSM (2009) Cardioprotective Effect of Gallic Acid on Cardiac Troponin-T, Cardiac Marker Enzymes, Lipid Peroxidation Products and Antioxidants in Experimentally Induced Myocardial Infarction in Wistar Rats. Chem Biol Interact 179: 118-124.

38. Geetha A, Sankar R, Marar T, Devi CS (1990) Alpha-Tocopherol Reduces Doxorubicin Induced Toxicity in Rats - Histological and Biochemical Evidences. Indian J Physiol Pharmacol 34: 94-100.

39. Devika PT, Prince PSM (2008) (−)Epigallocatechin-Gallate (EGCG) Prevents Mitochondrial Damage in Isoproterenol Induced Cardiac Toxicity in Albino Wistar Rats: A Transmission Electron Microscopic and in-vitro Study. Pharmacol Res 57: 351-357.

40. Polidoro G, Di Ilio C, Arduini A, La Rovere G, Federici G (1984) Superoxide Dismutase, Reduced Glutathione and TBA-Reactive Products in Erythrocytes of Patients with Multiple Sclerosis. Int J Biochem 16: 505-509.

41. Panda VS, Naik SR (2009) Evaluation of Cardioprotective Activity of Ginkgo biloba and Ocimum sanctum in Rodents. Altern Med Rev 14: 161-171.

42. Saravanan G, Ponmurugan P, Sathiyavathi M, Vadivukkarasi S, Sengottuvelu S (2013) Cardioprotective Activity of Amaranthus Viridis Linn: Effect on Serum Marker Enzymes, Cardiac Troponin and Antioxidant System in Experimental Myocardial Infarcted Rats. Int J Cardiol 165: 494-498.

43. Karthikeyan K, Bai BR, Devaraj SN (2007) Cardioprotective Effect of Grape Seed Proanthocyanidins on Isoproterenol Induced Myocardial Injury in Rats. Int J Cardiol 115: 326-333.

44. Zhou B, Wu LJ, Li LH, Tashiro SI, Onodera S, et al. (2006) Silibinin Protects against Isoproterenol Induced Rat Cardiac Myocyte Injury through Mitochondrial Pathway after Up-Regulation of SIRT1. J Pharmacol Sci 102: 387-395.

45. Meister A (1988) Glutathione Metabolism and its Selective Modification. J Biol Chem 263: 17205-17208.

46. Panda VS, Naik SR (2008) Cardioprotective Activity of Ginkgo biloba Phytosomes in Isoproterenol Induced Myocardial Necrosis in Rats: A Biochemical and Histoarchitectural Evaluation. Exp Toxicol Pathol 60: 397-404.

47. Corbi G, Conti V, Russomanno G, Longobardi G, Furgi G, et al. (2013) Adrenergic Signaling and Oxidative Stress: A Role For Sirtuins?. Front Physiol 4: 1-14.

48. Marchi E, Baldassari F, Bononi A, Wieckowski MR, Pinton P (2013) Oxidative Stress in Cardiovascular Diseases and Obesity: Role of p66Shc and Protein Kinase-C. Oxid Med Cell Longev.

49. Shah RA, Khan S, Rehman W, Vakil M (2016) Phytochemical Evaluation of Withanolide-A in Ashwagandha Roots from Different Climatic Regions of India. International Journal of Current Research in Biosciences and Plant Biology 3: 114-120.

50. Mathavi P, Nethaji S, Velavan (2015) GC-MS Analysis of Phytocomponents in the Methanolic Extract of Shorea robusta. International Journal of Science and Research 4: 1935-1938.

51. Razavi M, Nyamathulla S, Karimian H, Noordin MI (2014) Novel Swellable Polymer of Orchidaceae Family for Gastroretentive Drug Delivery of Famotidine. Drug Des Devel Ther 8: 1315-1329.

52. Kumar SB, Kumar VJ (2014) GC-MS Analysis of Bioactive Constituents from Cycas circinalis L. and Ionidium suffruticosum Ging. International Journal of Pharmaceutical Sciences Review and Research 28: 197-201.

53. Khanjian H, Schilling M, Maish J (2013) FTIR and Py-GC/MS Investigation of Archaeological Amber Objects from the J.Paul Getty Museum. e-PRESERVATION Science 10: 66-70.